

Dynamic effects in nonlinear magneto-optics of atoms and molecules: review

Evgeniy B. Alexandrov

A. F. Ioffe Physico-Technical Institute, 26 Polytekhnicheskaya, St. Petersburg 194021, Russia

Marcis Auzinsh

Department of Physics, University of Latvia, 19 Rainis Boulevard, Riga LV-1586, Latvia

Dmitry Budker

Department of Physics, University of California, Berkeley, California 94720, and Nuclear Science Division, Lawrence Berkeley National Laboratory, Berkeley, California 94720

Derek F. Kimball and Simon M. Rochester

Department of Physics, University of California, Berkeley, California 94720

Valeriy V. Yashchuk

Advanced Light Source Division, Lawrence Berkeley National Laboratory, Berkeley, California 94720

Received May 10, 2004; revised manuscript received August 17, 2004; accepted August 23, 2004

A brief review is given of topics relating to dynamical processes arising in nonlinear interactions between light and resonant systems (atoms or molecules) in the presence of a magnetic field. © 2005 Optical Society of America

OCIS codes: 020.0020, 270.1670.

1. INTRODUCTION

The study of resonant, nonlinear, magneto-optical effects (NMOE) is an active area of research with a rich history going back to the early work on optical pumping. These effects result from the resonant interaction of light with an atomic or molecular system in the presence of additional external electromagnetic fields (most commonly a uniform magnetic field, but we will also consider electric fields). A recent review by Budker *et al.*¹ deals primarily with the effects in atoms; the molecular case is detailed in a monograph by Auzinsh and Ferber.² In this paper, we focus on the dynamical aspects of such interactions, attempting to offer the reader a unified view on various diverse phenomena and techniques while avoiding excessive repetition of material already discussed in the previous reviews. Interest in the application of dynamic NMOE to experimental techniques has been increasing in recent years. The use of dynamic effects allows one to do things that are difficult with steady-state NMOE, for example, high-sensitivity, Earth-field-range magnetometry. Dynamic effects can also allow information (such as the value of energy-level splittings) that would normally be obtained from high-resolution spectroscopy to be extracted from direct measurements of frequency, a more robust technique.

NMOE (specifically those related to coherence phenomena¹) are observed when an optically polarized medium undergoes quantum beats (Section 2) under the influence of an external field, and so influences the polarization and/or intensity of a transmitted probe light beam. While this is inherently a dynamical process on the microscopic level, a macroscopic ensemble of particles³ reaches a steady state in about the polarization-relaxation time if the external parameters are held constant. Thus to observe quantum-beat dynamics, these parameters must be varied at a rate significant compared with the polarization-relaxation rate. One approach, discussed in Section 3, is to produce polarization with a pulse of pump light and then observe the effect of the subsequent quantum-beat dynamics on the optical properties of the medium. Alternatively, the method of beat resonances (Section 4) can be used in which an experimental parameter [the amplitude (Subsection 4.A), frequency (Subsection 4.B), or polarization (Subsection 4.C) of the light, the external field strength (Subsection 4.D), or the rate of polarization relaxation (Subsection 4.E)] is modulated and the component of the signal at a harmonic of the modulation frequency is observed. Resonances are seen when the modulation frequency is a subharmonic of one of the quantum-beat frequencies present in the system.

2. QUANTUM BEATS

Quantum beats^{2,4-7} is the general term for the time evolution of a coherent superposition of nondegenerate energy eigenstates at a frequency determined by the energy splittings. In this paper, we are primarily concerned with the evolution of a polarized ensemble of particles with a given angular momentum that have their Zeeman components split by an external field. For linear Zeeman splitting—the lowest-order effect due to a uniform magnetic field—the evolution is Larmor precession, i.e., rotation of the polarization about the magnetic field direction. For nonlinear splittings, such as quadratic Stark shifts, the polarization evolution is more complex. The state of the ensemble is described by the density matrix, which evolves according to the Liouville equation. While this is all that is necessary for a theoretical description of the system, physical insight can often be gained by decomposing the density matrix into polarization moments having the symmetries of the spherical harmonics. In quantum beats due to nonlinear energy splittings, the relative magnitudes of the various polarization moments change with time, a process sometimes known as alignment-to-orientation conversion (see Refs. 1, 2 and references therein). A pictorial illustration of the polarization state can be obtained by plotting its angular-momentum-probability distribution. The polarization-moment decomposition and angular-momentum-probability distribution not only aid physical intuition, but they are themselves complete descriptions of the ensemble state and can be used in some cases to simplify calculations. For a more detailed discussion, see Appendix A.

As an example we consider the nonlinear Zeeman shifts that occur when atoms with hyperfine structure are subjected to a sufficiently large magnetic field. For states with total electron angular momentum $J = 1/2$, such as in the alkali atoms, the shifted frequency ω_m of each Zeeman sublevel with spin projection m along the magnetic field direction is given by the Breit-Rabi formula⁷

$$\frac{\omega_m}{2\pi} = -\frac{\Delta}{2(2I+1)} - g_I\mu m B \pm \frac{\Delta}{2} \left(1 + \frac{4m\xi}{2I+1} + \xi^2 \right)^{1/2}, \quad (1)$$

where $\xi = (g_J + g_I)\mu B/\Delta$; g_J and g_I are the electronic and nuclear Landé factors, respectively; B is the magnetic field strength; μ is the Bohr magneton; Δ is the hyperfine-structure interval; I is the nuclear spin; and the \pm sign refers to the upper and the lower hyperfine level, respectively. We set $\hbar = 1$ throughout this paper.

Consider an atomic sample of Cs ($I = 7/2$) initially in a stretched state ($m_z = F = 4$) with respect to the z axis. In the presence of an \hat{x} -directed magnetic field, the energy eigenstates are the $|Fm_x\rangle$ eigenstates of the F_x operator. The stretched state along \hat{z} is a superposition of these nondegenerate eigenstates, so quantum beats are seen in the evolution of the system.

The time evolution of each eigenstate is given by $c_m \exp(-i\omega_m t)|Fm\rangle$, where c_m is the initial amplitude. For moderate field strengths such that the parameter ξ is small, the shifts deviate only slightly from linearity. Thus expanding Eq. (1) in powers of ξ , we see that over

time scales comparable to the Larmor period, the evolution (to first order) is just Larmor precession with period $\tau_1 \approx 8(g_J\mu B)^{-1}$ (neglecting here g_I compared with g_J). The evolution due to the second-order quadratic shifts is also periodic, but with a much longer period $\tau_2 \approx 32\Delta(g_J\mu B)^{-2}$. (For $B = 0.5$ G, $\tau_1 \approx 6$ μ s, and $\tau_2 \approx 0.3$ s.) One way to illustrate these quantum beats is to produce graphs of the spatial distribution of angular momentum at a given time. To do this, we plot three-dimensional closed surfaces for which the distance from the origin in a given direction is proportional to the probability of finding the maximum projection of angular momentum along that direction.^{8,9} This plot illustrates the symmetries of the polarization state, indicating which polarization moments are present. (For a discussion of the angular-momentum-probability distribution and the polarization moments, see Appendix A.) A collection of surfaces showing the time evolution of the polarization over half a period τ_2 of the second-order evolution is shown in Fig. 1. The first plot (top left) represents the initial stretched state—the surface is stretched in the \hat{z} direc-

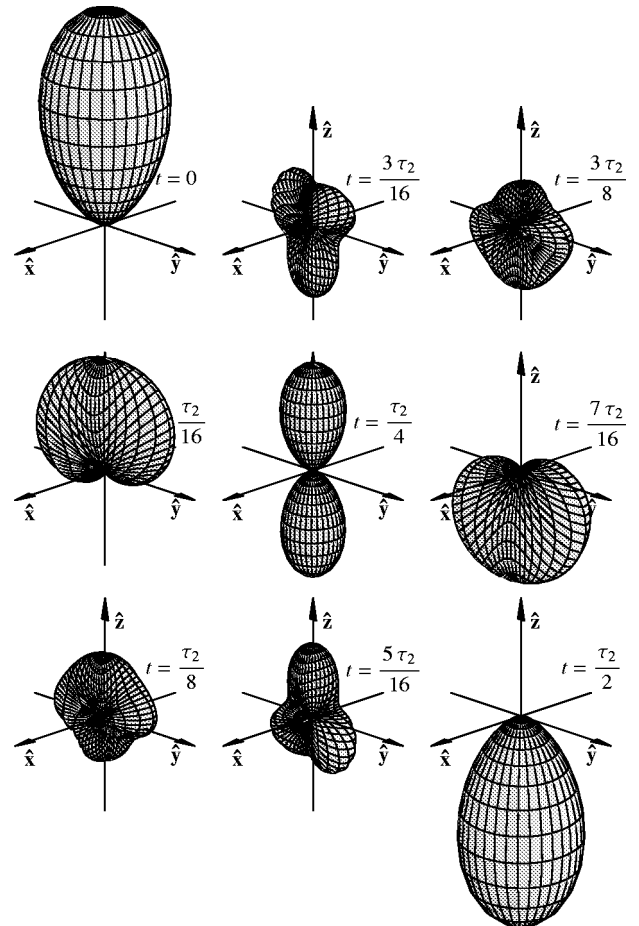


Fig. 1. Quantum beats in Cs illustrated with surfaces representing the probability of finding the system in the state with maximal projection $m = F$ in a given direction.^{8,9} This sequence is “stroboscopic” in the sense that the surfaces correspond to times chosen to have the same phase of the fast Larmor precession around the direction of the magnetic field \hat{x} . From the symmetry of the plots one clearly sees that orientation present in the initial state collapses and revives in the process of the temporal evolution. Temporal variation of higher polarization moments gives rise to higher-order-symmetry contributions to the probability surface (see also Fig. 3).

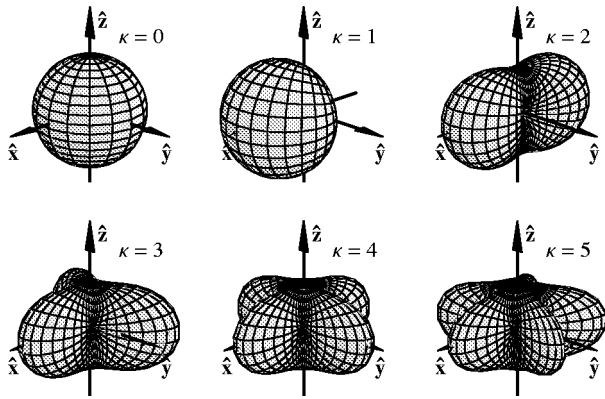


Fig. 2. Angular momentum spatial distribution for states composed only of population (ρ_0^0) and the maximum possible values of the components $\rho_{\pm\kappa}^{\kappa}$ for a particular κ . $\kappa = 0$, monopole moment (isotropic state with population only); $\kappa = 1$, dipole moment (oriented state); $\kappa = 2$, quadrupole moment (aligned state); $\kappa = 3$, octupole moment; $\kappa = 4$, hexadecapole moment; $\kappa = 5$, triakontadipole moment.

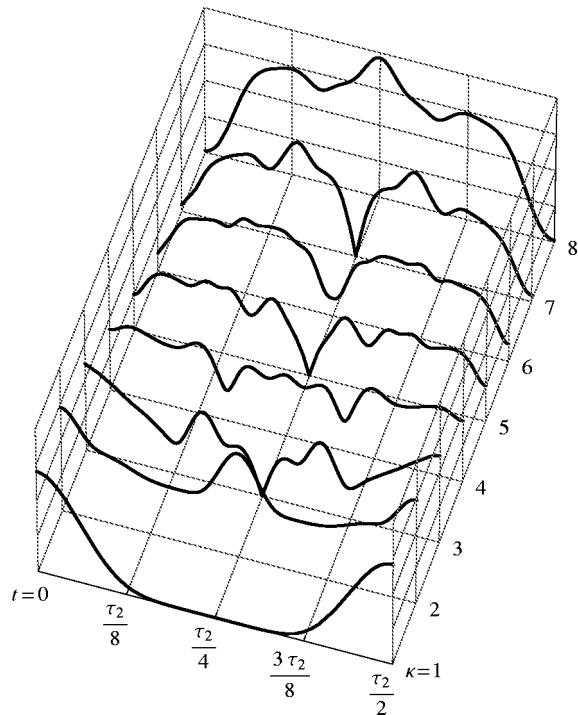


Fig. 3. Temporal evolution of the norms of various polarization moments of ranks κ of the $F = 4$ ground state of Cs corresponding to the case of Figs. 1 and 4. The initial stretched state is dominated by the lowest-order moments; at $t = \tau_2/4$ the state is composed only of even-order moments.

tion. This state undergoes rapid precession around \hat{x} of period τ_1 . At the same time, the slower second-order evolution results in changes in the shape of the probability surface. By “stroboscopically” drawing successive surfaces each at the same phase of the fast Larmor precession (i.e., at integer multiples of τ_1), we can see the polarization evolve into states with higher-order symmetry before becoming stretched along $-\hat{z}$ at $t = \tau_2/2$. In particular at $t = \tau_2/4$ the state is symmetric with respect to the x - y plane, a characteristic of the even orders in the decomposition of the polarization state into irreducible

tensor moments ρ^{κ} (see Appendix A). In general for a multipole moment of rank κ with polarization transverse to the quantization axis (such that only the components ρ_q^{κ} with $q = \pm\kappa$ are nonzero) this moment has rotational symmetry of order κ about that axis^{2,10} (see Fig. 2).

To explore the decomposition into polarization moments further, it is useful to plot the norms⁹ of the polarization moments as a function of time (see Fig. 3). The figure shows that initially the lowest-order moments predominate. At $t = \tau_2/4$ the odd-order moments are zero and the state comprises even-order moments only.

We can now connect these pictures of the atomic polarization state to an experimentally observable signal, e.g., the absorption of weak, circularly polarized light propagating along \hat{z} . To find the absorption coefficient, assuming that the upper-state hyperfine structure is not resolved, we transform to the $|J, m_J\rangle|I, m - m_J\rangle$ basis with quantization axis along \hat{z} and sum over the transition rates for the Zeeman sublevels. At short time scales [Fig. 4(a)] we see absorption modulated at the Larmor frequency as the result of precession of the atomic polarization about the x axis. The absorption is minimal when the state is oriented along \hat{z} and maximal when it is oriented along $-\hat{z}$. Looking at the envelope of this modulation at longer time scales, we see collapse and revival with period $\tau_2/2$ of the absorption oscillation amplitude [Fig. 4(b)]. The maxima of the envelope are associated with the stretched states shown in Fig. 1 and the minima with the states that are symmetric with respect to the x - y plane. This can also be seen by comparison with Fig. 3; the envelope of the signal plotted in Fig. 4(b) is proportional to the norm of the $\kappa = 1$ moment (orientation), and does not have any of the time-dependent behavior exhibited by the higher-order moments in Fig. 3. While it is true in general that weak probe light is not coupled to

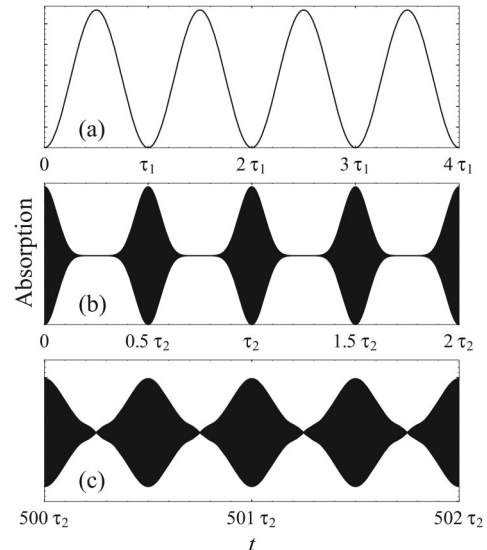


Fig. 4. Collapse and revival beats arising in optically pumped Cs atoms as a result of nonlinearity of Zeeman shifts. (a) Time-dependent absorption of the probe light (see text) observed on a short time scale reveals an oscillation at the Larmor frequency. (b) Observation on a longer time scale reveals the characteristic collapse and revival (beating) behavior. Note period of essentially complete collapse of the oscillation pattern. (c) At even longer time scales, the beat pattern is modified as a result of third-order nonlinearity.

atomic polarization moments of rank greater than two,¹¹ the fact that the absorption is insensitive to the $\kappa = 2$ moment (alignment) is a consequence of our assumption that the upper-state hyperfine structure is unresolved. In Fig. 4(c) one can see the effect of the third-order terms in the expansion of Eq. (1), reducing the contrast of the envelope function.

Collapse and revival phenomena similar to the effect described here have been observed in nuclear precession.¹² In that work spin precession of an $I = 3/2$ system in ²⁰¹Hg was studied, and the slight deviations from linearity in the Zeeman shifts responsible for the collapse and revival beats were due to quadrupole-interaction shifts arising from the interaction of the atoms with the walls of a rectangular vapor cell. Collapse and revival phenomena in molecules with large angular momenta were considered in a tutorial paper.¹³

3. TRANSIENT DYNAMICS

To observe macroscopic dynamics in magneto-optical effects, some experimental parameter must be varied in time. Perhaps the most conceptually straightforward technique is to induce atomic or molecular polarization with a pulse of pump light and then observe the transient response. Quantum beats were originally observed in this way by detecting fluorescence.^{14,15} We are primarily concerned here with techniques involving probe-light detection (a brief discussion of fluorescence experiments is given in Subsection 6.A). An early application of this method in conjunction with probe-light-polarization spectroscopy was an experiment¹⁶ with Yb vapor. A 5-ns pulse of linearly polarized, dye-laser light produced a coherently excited population in the 6^3P_1 state whose Zeeman sublevels were split by a magnetic field. The transmission of a subsequent linearly polarized, probe-light pulse was observed through a crossed polarizer. Optical anisotropy in stimulated emission was observed as polarization rotation of the probe beam. The time dependence of the signal due to the quantum-beat evolution (Larmor precession) of the excited-state polarization was investigated indirectly by holding the probe-pulse delay time τ fixed and sweeping the magnetic field. Oscillations corresponding to $\cos 2\Omega_L\tau$, where Ω_L is the Larmor frequency, were seen in the signal. The factor of two appears because linearly polarized light induces alignment (the $\kappa = 2$ tensor moment) that has twofold symmetry about any axis perpendicular to the alignment axis (Section 2). Thus the quantum-beat frequency for this moment is $2\Omega_L$; in general a rank- κ moment polarized as shown in Fig. 2 will have quantum-beat frequency $\kappa\Omega_L$ in a \hat{z} -directed magnetic field.

Recently, nonlinear magneto-optical rotation with pulsed pump light was used to study the sensitivity limits of atomic magnetometry at very short time scales.^{17,18} Observation of the time dependence of optical rotation of a weak probe beam allows the measurement of the magnetic field to be corrected for the initial spin-projection uncertainty. For measurement times T short enough that non-light-induced, polarization-relaxation processes can be neglected (in this case $T \ll (\gamma\sqrt{N})^{-1}$, where γ is the relaxation rate and N is the number of polarized at-

oms), a “quantum nondemolition measurement”¹⁹ can be performed by using far-detuned probe light. Over this time a subshot-noise measurement with uncertainty scaling as $N^{-3/4}$ is then possible.²⁰ If squeezed light¹⁹ is used Heisenberg-limited scaling of N^{-1} can be obtained limited to an even shorter measurement time $T \ll (\gamma N)^{-1}$.

In the experiments discussed so far in this section, the measurement times were much shorter than the polarization-relaxation time. When longer measurements are made, the amplitude of the quantum beats will be seen to decay during the measurement as a result of mechanisms such as collisional relaxation and, for excited states, spontaneous emission.²¹ An often important mechanism that has the effect of polarization relaxation is fly through or transit relaxation. This results from polarized particles traveling out of the probe light beam while unpolarized particles enter the beam, resulting in a decrease in average polarization in the probe region. The effective rate of this relaxation γ_t can be estimated from the average thermal velocity over the size of the relevant region. However, this relaxation is in general *not* described by an exponential decay with time constant γ_t , but in many cases can be substantially more complicated. For example, consider a situation in which, immediately after the pump pulse, particles are polarized in a spatial region that is larger than the probe region. This can occur even if the pump and probe beams have identical and overlapping profiles under conditions of nonlinear absorption: A strong Gaussian-profile pump beam can perform efficient optical pumping even far away from the beam center. The weak probe, on the other hand, acts at the intensity range of linear absorption; it takes some time for particles in thermal motion to reach the beam center where they undergo the probe interaction. As a result in the initial moments following the pump pulse, one does not observe significant effective relaxation. Only after a certain amount of time does fly-through relaxation set in. This effect was predicted and measured for relaxation of ground-state K_2 molecules.²² This nonexponential relaxation kinetics can be significant in the quantitative analysis of quantum-beat signals.

In addition to the observation of transients, another way to study quantum-beat dynamics is to use resonance techniques involving modulation of the external experimental conditions. Such techniques are discussed in Section 4.

4. BEAT RESONANCES

A. Amplitude Resonances

In a pulsed experiment such as those described in Section 3, the quantum beats will tend to wash out as the pulse rate is increased relative to the polarization-relaxation rate. Particles polarized during successive pulses will, in general, beat out of phase with each other, canceling out the overall medium polarization. If the quantum-beat frequency is slower than the relaxation rate, each polarized particle will not be able to undergo an entire quantum-beat cycle before relaxing. Thus the quantum beats will not cancel completely, and there will be some residual steady-state polarization. This is the effect studied in the limiting case of steady-state NMOE experi-

ments with cw pump light. If the quantum-beat frequency is faster than the relaxation rate, each particle will contribute to the average polarization over its entire quantum-beat cycle, and the macroscopic polarization of the medium will be destroyed entirely. This is the reason that magnetometers based on steady-state NMOE lose sensitivity for Larmor frequencies greater than the relaxation rate. However, time-dependent, macroscopic polarization can be regained—even for high quantum-beat frequencies—if the pump light is pulsed or amplitude modulated at a subharmonic of the quantum-beat frequency.²³ Polarization is produced in phase with that of particles pumped on previous cycles. The light pulses contribute coherently to the medium polarization, and the ensemble beats in unison. This effect is known as synchronous optical pumping or “optically driven spin precession.”^{26,27} This is a particular case of a general class of phenomena known as beat resonances^{2,7,14,28} exhibited when a parameter of the pump light or external field is modulated, as discussed below. In NMOE experiments such resonances are generally observed by using lock-in detection of the transmission or polarization signal of the probe light at a harmonic of the modulation frequency. However, in some cases, such as when total transmission (or fluorescence) is observed, the resonances can also be detected in the time-averaged signal.²⁹

In 1961, Bell and Bloom²⁶ were the first to observe beat resonances due to quantum beats in the ground states of Rb and Cs and in metastable He. The first ground-state, quantum-beat resonance experiments in molecules were performed with Te₂³⁰ and were followed by experiments with K₂.^{31,32} Synchronous optical pumping has been used over the years in many applications. To give just one example, this method was employed in sensitive searches^{33–35} for a possible permanent electric-dipole moment (whose existence is possible only as a result of a violation of both parity and time-reversal invariance) of ¹⁹⁹Hg.

B. Frequency Resonances

Frequency (rather than amplitude) modulation of the pump light can be used to produce an effect similar to that discussed in Subsection 4.A. Here the optical pumping rate is modulated as a result of its frequency dependence. One example of this is nonlinear magneto-optical (Faraday) rotation with frequency-modulated light (FM NMOR).^{36–38} In this technique linearly polarized light near-resonant with an atomic transition is directed parallel to the magnetic field. The frequency of the light is modulated, causing the rates of optical pumping and probing to acquire a periodic time dependence. As described in Subsection 4.A a resonance occurs when the quantum-beat frequency $\kappa\Omega_L$ for a rank- κ polarization moment equals the modulation frequency Ω_m (the lowest-order nonisotropic polarization moment here has $\kappa = 2$). The atomic sample is pumped into a macroscopic, rotating, polarized state that causes a periodic modulation of the plane of light polarization at the output of the medium. The amplitude of time-dependent optical rotation at various harmonics of Ω_m can be measured with a phase-sensitive lock-in detector (Fig. 5). Additional resonances can be observed when the quantum-beat frequency is equal to higher harmonics of the modulation

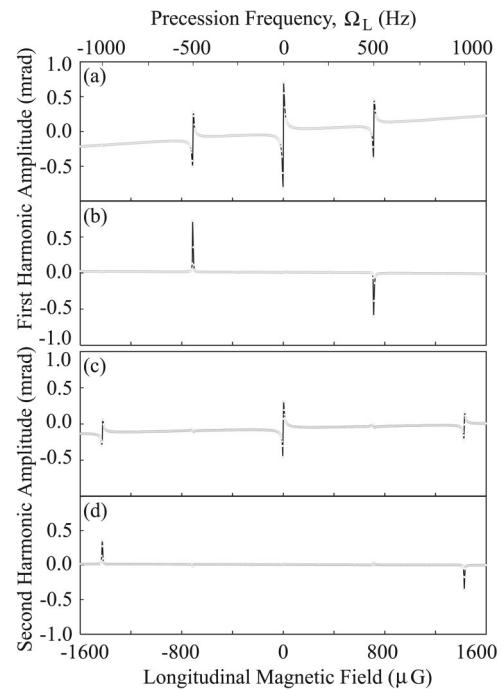


Fig. 5. Signals detected at the first harmonic (a), (b) and second harmonic (c), (d) of Ω_m as a function of longitudinal magnetic field. This experiment employed buffer-gas-free, paraffin-coated vapor cells containing isotopically enriched ⁸⁷Rb. The laser was tuned near the *D*1 line, laser power was 15 μ W, beam diameter ~ 2 mm, $\Omega_m = 2\pi \times 1$ kHz, and the modulation amplitude $\Delta\omega_m = 2\pi \times 220$ MHz. Traces (a), (c) and (b), (d) correspond to the in-phase and the quadrature outputs of the signals from the lock-in detector, respectively. The zero-field resonances observed in traces (a), (c) are similar in nature to the resonances observed in static NMOE studies (see text). The quadrature components arise because of a phase difference between the “probe” modulation and the modulation of the optical properties of the atomic medium. (Aligned atoms produce maximum optical rotation when the alignment axis is at an angle of $\pi/4$ to the light-polarization direction.) Figure from Ref. 36.

frequency (or what is equivalent, Ω_m is equal to subharmonics of the beat frequency $2\Omega_L/n$, where n is the harmonic order).

As discussed in Subsection 4.A, in a steady-state, NMOR experiment, the equilibrium polarization of the ensemble depends on the balance of Larmor precession with various mechanisms causing the polarization to relax (e.g., spin-exchange collisions or wall collisions). When the Larmor frequency is much less than the relaxation rate, the magnitude of the optical rotation increases linearly with the Larmor frequency. When the Larmor frequency increases, polarization is washed out and optical rotation falls off. Such zero-field resonances are also observed in the magnetic field dependence of the in-phase FM NMOR signals (Fig. 5). For the zero-field resonances Ω_m is much faster than both Ω_L and the optical pumping rate for the cell, so the frequency modulation does not significantly affect the pumping process. On the other hand, as the laser frequency is scanned through resonance, there arises a time-dependent optical rotation, so the signal contains various harmonics of Ω_m .

The FM NMOR technique is useful for increasing the dynamic range of NMOR-based magnetometers (Subsection 5.B). The beat resonances have width comparable

with that of the zero-field resonance (since the dominant relaxation mechanisms are the same) but in principle can be centered at any desired magnetic field.

C. Polarization Resonances

In addition to beat resonances obtained by modulation of the light amplitude and frequency, resonances due to modulation of light polarization have also been studied (for a review of earlier work see Ref. 39). These polarization resonances (also called phase resonances) are much like the other light modulation effects discussed above. Polarization modulation can be thought of as out-of-phase amplitude modulation of the light polarization components, providing a conceptual link to amplitude resonances (Subsection 4.A).

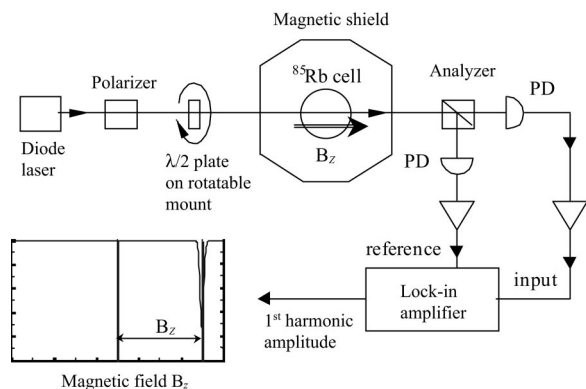


Fig. 6. Experimental arrangement for the polarization resonance study.

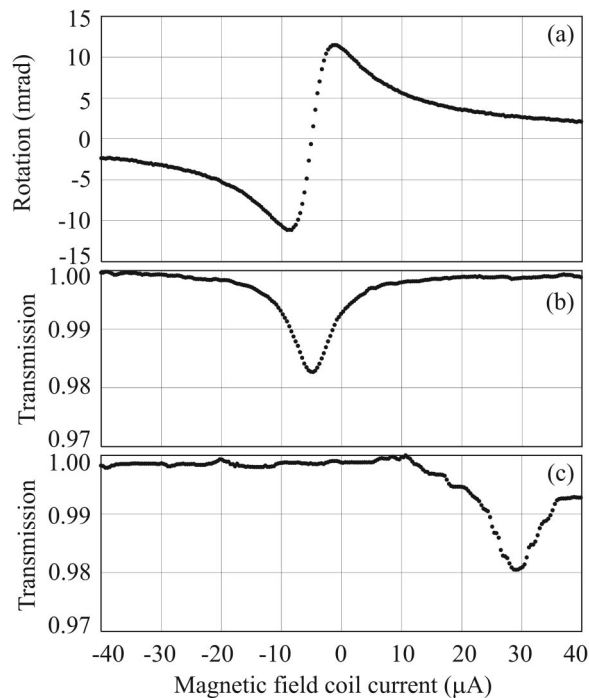


Fig. 7. Faraday rotation angle (a) and transmission (b) dependences on magnetic field recorded with stationary linear polarization of light. Trace (c) shows light transmission as a function of magnetic field when the linear polarization is rotated at $\Omega_m = 2\pi \times 14$ Hz. Coil current of $1 \mu\text{A}$ corresponds to a magnetic field of approximately $1 \mu\text{G}$.

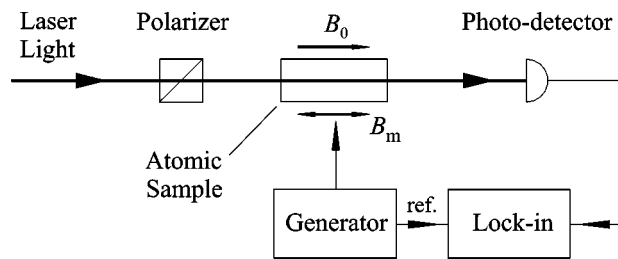


Fig. 8. Schematic of an experimental arrangement for parametric-resonance spectroscopy with magnetic field modulation.

For Zeeman beats the light polarization, when rotated at the Larmor frequency, is always parallel to the alignment of the ensemble. In this case, optical pumping contributes continuously and coherently to a rotating, aligned polarization state of the ensemble. This effect was studied in an experiment⁴⁰ with Rb. A $\lambda/2$ -plate on a motor-driven rotating optical mount was used to rotate the light polarization direction continuously at a fixed frequency; transmission was observed with lock-in detection at this frequency while the longitudinal magnetic field strength was swept (Fig. 6). The “dark resonance,” a drop in transmission, is normally centered at zero field when light polarization is fixed [Fig. 7(b)]. This resonance was shifted by the polarization-rotation frequency [Fig. 7(c)]. Polarization resonances occurring in molecules have been analyzed theoretically.²⁹ In that work, the time-averaged fluorescence intensity was considered as the method of detection.

D. Parametric Resonances

As mentioned in Subsection 4.A one way to obtain beat resonances is to modulate the external field (e.g., the magnetic field) and consequently the Larmor precession frequency. This method has been used for sensitive atomic magnetometry⁴¹ and is presently employed as a useful general-nonlinear-spectroscopic technique⁴² known as parametric resonance. In a typical setup (Fig. 8), linearly polarized, resonant laser light traverses the medium to which a magnetic field parallel to the light-propagation direction is applied. The magnetic field has two components—a nearly dc component (that can be slowly scanned) and an ac component with frequency much higher than the ground-state, polarization-relaxation rate. Transmitted light intensity is monitored with a photodetector, the signal from which is analyzed with a lock-in amplifier referenced to the ac modulation of the magnetic field.

As in FM NMOR (Subsection 4.B, Fig. 5) there are two types of resonances that are seen when the dc magnetic field is scanned: the zero-field resonance (independent of the ac-modulation frequency) that appears only in the in-phase component of the signal and the frequency-dependent resonances in both the in-phase and quadrature components. The former arises because for resonant light the transmission is a quadratic function of the magnetic field, while the latter are due to an effective modulation of the rate of polarization production. As the ac field adds to or subtracts from the static field, it leads to acceleration or deceleration of the Larmor precession,

respectively. Since as discussed in Subsection 4.A Larmor precession acts to average out the macroscopic polarization induced by cw pump light, more overall polarization is generated when the Larmor precession rate is the slowest. As a result the rate of polarization production is modulated at the ac frequency, and so, as for amplitude or frequency resonances, a beat resonance occurs when the modulation frequency is a subharmonic of the quantum-beat frequency.

E. Parametric Relaxation Resonances

Beat resonances can also arise when the parameter that is modulated is the relaxation rate of the atomic polarization. Here again resonances occur when the frequency of the modulation coincides with the spin-precession frequency or its subharmonic. This effect was predicted theoretically^{43,44} and observed experimentally⁴⁵ in metastable He where the relaxation rate was modulated by modulating the discharge current in a He cell. Note that since relaxation is independent of the direction of the atomic spins (isotropic relaxation), this method, in contrast to those discussed above, cannot produce large overall polarizations of the sample when the Larmor precession rate significantly exceeds the relaxation rate (see Subsection 4.A).

We also briefly mention here another related dynamic magneto-optical effect: A sudden change in the relaxation or optical pumping rate for a driven spin system can cause transient spin nutations⁴⁶ while the system relaxes towards its new equilibrium state.

F. Relation to Coherent Population Trapping

An equivalent description of the beat-resonance phenomena can be given in terms of coherent population trapping (CPT), an effect that is also closely related to Λ resonances and mode crossing (see Ref. 47 for a review). Indeed, harmonic modulation of the light intensity leads to the appearance of two sidebands at frequencies shifted from the unperturbed light frequency ω_0 by the value of the modulation frequency: $\omega_{1,2} = \omega_0 \pm \Omega_m$. With modulation depth less than 100%, the spectral component with frequency ω_0 also survives [Fig. 9(a)]. A CPT resonance occurs when the frequency difference between a pair of spectral components of the modulated light coincides with the frequency splitting of the lower-state Zeeman sublevels, so that light is resonant with a pair of transitions.⁴⁷ For a $F = 1 \rightarrow F' = 0$ transition [Fig.

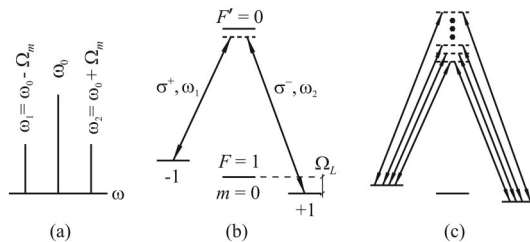


Fig. 9. (a) Light frequency spectrum for light-intensity modulation with 50% depth. (b) CPT resonance at double modulation frequency in the case of a $F = 1 \rightarrow F' = 0$ transition. The lower state Zeeman sublevels are split in a magnetic field applied along the quantization axis. (c) CPT resonances in the case of frequency modulation with a large modulation index.

9(b)], a CPT resonance leads to transfer of population from the “bright” state to the “dark” states that are uncoupled to the light, and light transmission increases. For harmonic modulation of the light intensity there are two spectral difference frequencies ($\Omega_m, 2\Omega_m$), each resulting in an observed resonance²⁶ when the difference becomes equal to $2\Omega_L$, the splitting between the $M = 1$ and $M = -1$ energy levels.

CPT resonances can also occur when the light is frequency modulated. In this case the light spectrum consists of an infinite number of sidebands with amplitudes of the n th sideband given by a Bessel function $J_n(m)$ corresponding to the modulation index $m = \Delta\omega_m/\Omega_m$, where $\Delta\omega_m$ is the modulation depth. For example, an experiment⁴⁸ with Cs atoms studied the application of the CPT effect with frequency-modulated light to atomic magnetometry. The value of the modulation index was $m \approx 1.5$, so only a few sidebands were prominent. Both vacuum and buffer-gas cells were used, and the minimum observed width of the CPT resonance was 1.4 kHz in the latter case. The width of the resonance sets the lower bound on the magnetic fields (and correspondingly the resonance frequency) for which the resonances can be resolved.

The situation changes somewhat if the modulation index becomes large. For example in the FM NMOR experiments described in Subsection 4.B the modulation depth is $\Delta\omega_m \approx 30$ MHz and the modulation rate is $\Omega_m \approx 100$ – 1000 Hz.^{36–38} Thus $m \approx 10^5$ and the pairs of $\Delta M = 2$ sublevels are coupled by a very large number of frequency–sideband pairs with comparable amplitude [Fig. 9(c)]. For this reason the description in terms of the CPT resonances is less intuitive here than the synchronous-pumping picture presented in Subsection 4.B.

5. APPLICATIONS

A. High-Order Polarization Moments

The use of Zeeman-beat resonances allows one to directly create and detect higher-order polarization moments. Because a rank κ moment with polarization transverse (in the sense described in Section 2) to the magnetic field axis has symmetry of order κ about that axis, a resonance in both pumping and probing due to interaction with this moment occurs when the light–particle interaction is modulated at the frequency $\Omega_m = \kappa\Omega_L$. A dipole transition can connect polarization moments with ranks differing by at most two. Consequently, multiple photon interactions are required to generate high-rank polarization moments. For example, two interactions are required to produce a rank $\kappa = 4$ hexadecapole moment from an initially unpolarized ($\kappa = 0$) state. There must be an equal number of photon interactions to detect a signal due to the high-order multipole moment, which will be modulated at $\kappa\Omega_L$. Thus the amplitude of the signal due to the hexadecapole resonance scales as the fourth power of the light intensity, as experimentally observed³⁷ in FM NMOR (Subsection 4.B).

Figure 10 shows the magnetic field dependence of FM NMOR signals from a paraffin-coated cell containing ^{87}Rb in which the atoms are pumped and probed with a single

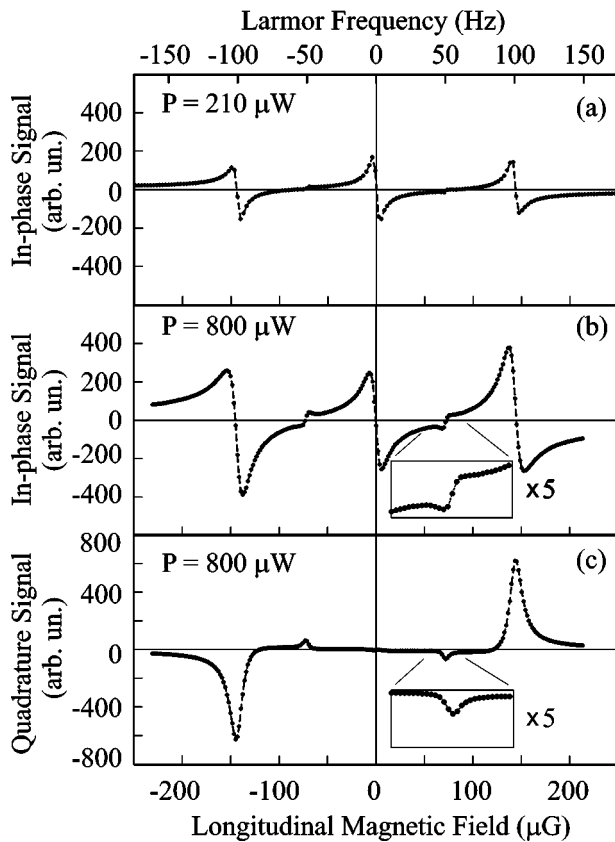


Fig. 10. Example of the magnetic field dependence of the FM NMOR signals showing quadrupole resonances at $B = \pm 143.0 \mu\text{G}$ and hexadecapole resonances at $\pm 71.5 \mu\text{G}$. Laser modulation frequency is 200 Hz, modulation amplitude is 40 MHz peak-to-peak; the central frequency is tuned to the low-frequency slope of the $F = 2 \rightarrow F' = 1$ absorption line. Plots (a), (b) show the in-phase component of the signal at two different light powers; plot (c) shows the quadrature component. Note the increase in the relative size of the hexadecapole signals at the higher power. The insets show zooms on hexadecapole resonances. Figure from Ref. 37.

light beam tuned to the $D1$ transition. At relatively low light power [Fig. 10(a)], there are three prominent resonances: one at $B = 0$ and two corresponding to $2\Omega_L = \Omega_m$ (see Subsection 4.B, Fig. 5). Much smaller signals whose relative amplitudes rapidly grow with light power are seen at $4\Omega_L = \Omega_m$, the expected positions of the hexadecapole resonances.

Various experimental signatures of high-rank polarization moments were previously detected with other techniques,^{49–55} but by taking advantage of the unique periodicity of the dynamic optical signals with beat resonances, such high-rank moments can be directly created, controlled, and studied. Because of the enhanced optical nonlinearities and different relaxation properties, higher-order polarization moments are of particular interest for application in many areas of quantum and nonlinear optics. In addition, when performing high-field magnetometry in alkali atoms (Subsection 5.B), the use of the highest-order polarization moment supported by a given state may be advantageous, because its evolution is free of complications due to nonlinear dependence of the Zeeman shifts on the magnetic field.³⁷

B. Magnetometry

The steady-state NMOE are a valuable tool for magnetometry; it has been shown⁵⁶ that the sensitivity of a magnetometer based on nonlinear Faraday rotation can reach $\sim 10^{-11} \text{ GHz}^{-1/2}$. Dynamic techniques can provide useful extensions to the steady-state methods—in particular they can be used to increase the magnetometer's dynamic range by translating the narrow zero-field resonances to higher magnetic fields. As discussed in Subsection 4.B steady-state NMOE lose sensitivity to magnetic fields when the Larmor frequency is greater than the polarization-relaxation rate. If beat resonances are used for magnetic field detection, however, the dependence of the resonance condition on the modulation frequency can be used to tune the response of the system to a desired magnetic field range.

While the earliest examples of beat-resonance magnetometry used amplitude²⁶ or parametric^{41,57} resonances, in recent years the use of light-frequency modulation has become more common.^{36,58–60} This is a result of the development and broad use of single-mode, diode-laser systems. For such lasers frequency modulation through the diode current and/or the cavity length controlled with a piezoelectric transducer voltage can be simpler and more robust than either light-amplitude modulation or modulation of the applied magnetic field. However, such frequency modulation is usually accompanied by intensity modulation of up to $\sim 15\%$.⁶⁰ The deleterious effects of parasitic modulation and of laser-intensity noise can be avoided by detecting optical rotation³⁶ rather than transmission.

The use of beat resonances to selectively address high-rank polarization moments (Subsection 5.A) can also be an advantage in magnetometry. Detection of such polarization moments may result in increased statistical sensitivity by allowing the use of higher light power without significant increase in the polarization-relaxation rate due to power broadening.³⁷

One possible application of beat-resonance magnetometers is to low-field and remote-detection nuclear magnetic resonance and magnetic-resonance imaging. Both parametric resonance⁵⁷ and FM NMOR magnetometers⁶¹ have been used to measure the nuclear magnetization of a gaseous sample placed near a “probe” Rb-vapor cell. In the latter work, the fields—due to Xe that was polarized by spin-exchange collisions with laser-polarized Rb—were in the nanogauss range.

6. RELATED TOPICS

A. Fluorescence Detection

Another standard technique for the observation of quantum beats is the detection, not of polarization or transmission of a probe beam, but of spontaneous emission from an excited state. Quantum beats in fluorescence induced by weak probe light after pulsed excitation were observed for the first time in an experiment^{62,63} measuring the magnetic moment of the ($v'' = 1, J'' = 73$) rovibronic level of the ground electronic state $X^1\Sigma_g^+$ of K_2 molecules. Many molecules have $^1\Sigma$ ground states. The magnetic moment of these states is nominally zero—nonzero cor-

rections appear only because of mixing with other states due to perturbation by molecular rotation.⁶⁴ This makes calculations of magnetic moments in $^1\Sigma$ states rather complicated, and experimental measurements of these moments become important.

As noted in Subsection 5.A, a single-photon dipole interaction couples polarization moments with a difference in rank of $\Delta\kappa \leq 2$. Since the absorption and re-emission of probe light is a two-photon process, moments up to rank four can be observed in fluorescence induced by single-photon excitation. Indeed, excited-state alignment will be directly connected by a dipole transition to all existing ground-state moments from population ($\kappa = 0$) to the hexadecapole moment ($\kappa = 4$). This technique was used in the study of the K_2 ground state for the first observation^{31,32,65} of a beat resonance due to the hexadecapole moment (Fig. 11). Relaxation dynamics²² and Zeeman beats⁶³ of multipole moments up to hexadecapole in K_2 molecules were also observed using pulsed pump light and fluorescence detection.

So far, we have discussed quantum beats arising as a result of the temporal evolution of the ground state. Obviously one can also detect quantum beats in excited-state dynamics by observing fluorescence after pulsed excitation. This technique was used for the first observations of quantum beats in atoms in experiments with the 6^3P_2 state¹⁴ of Hg and the 5^3P_1 state¹⁵ of Cd. In diatomic molecules quantum beats from an excited state were first observed⁶⁶ with I dimers in the $B^3\Pi_{0_u^+}$ state.

Quantum-beat studies measuring fluorescence from metastable states have been done as part of efforts to improve the present-day limit⁶⁷ on the parity- and time-reversal-invariance-violating, permanent electric-dipole moment (EDM) of the electron.⁶⁸ Close-lying states of opposite parity that can be mixed by a static electric field are advantageous for EDM measurements. The $J = 1$ level of the first electronic excited state of lead oxide (PbO), $a(1)[^3\Sigma^+]$, is split into two opposite-parity states (the Ω doublet⁶⁹) separated by only ≈ 11 MHz. A recent experiment⁷⁰ studied quantum beats in fluorescence from

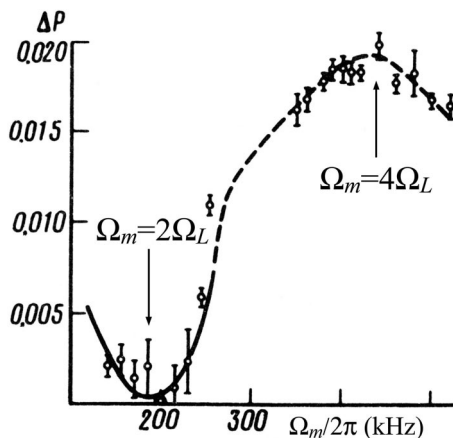


Fig. 11. Ground-state beat-resonance signal measured as a change of the degree of polarization of laser-induced fluorescence as a function of modulation frequency Ω_m of excitation light. The experiment was done with K_2 molecules. Two resonances were observed at twice (alignment) and four times (hexadecapole moment) the Larmor frequency Ω_L . Figure from Ref. 65.

molecules excited by a dye-laser pulse to the $J = 1$ states of $a(1)(v' = 5)$. For an EDM measurement it is necessary to measure small shifts with great accuracy; a sensitivity of $\approx 50 \text{ Hz}/\sqrt{\text{Hz}}$ was demonstrated,⁷⁰ consistent with shot-noise in the experiment. Precision measurements of the Landé factors of the two components of the Ω doublet were also made, laying the groundwork for a future EDM measurement. Quantum-beat measurements have also been done in atoms to evaluate metastable states for use in an EDM measurement: precision tensor polarizability measurements were done with Stark-induced quantum beats in Sm.⁷¹ Also, a pair of long-lived, opposite-parity states in Dy that are separated by only 3 MHz were studied.⁷² These states, components of which can be brought to crossing by applying a weak static magnetic field, were used in a quantum-beat technique to search for effects of parity violation.⁷³

B. Polarization-Noise Spectroscopy

An unpolarized medium clearly can not produce a net quantum-beat signal. However, even in an unpolarized sample the randomizing processes that relax polarization at a rate γ cause the medium polarization to fluctuate around its average value of zero. Since polarization created at a given time persists for an average time $1/\gamma$, the polarization-noise spectrum contains components only at frequencies less than $\sim \gamma$ in the absence of an external field. When a magnetic field is applied, the polarization produced at a given time undergoes quantum beats, and so the detected signal in probe light propagating along the magnetic field direction is modulated at the quantum-beat frequency. Thus the peak in the noise spectrum originally centered at zero frequency with width γ is shifted to the quantum-beat frequency. This effect has been observed for Zeeman beats in an experiment on the 589-nm resonance line of Na contained in a vapor cell with buffer gas.⁷⁴

While the effect described above is classical in the sense that it is not related to the inherent uncertainty in the polarization of each individual particle, quantum effects can also be relevant. In particular, the uncertainty relation between Cartesian components of the angular momentum implies that a similar polarization-noise effect can be present not only for unpolarized samples, but even when there is full polarization. For example, the noise would still be present in the same experimental geometry if the particles were fully polarized along the magnetic field and had no longitudinal relaxation. The width of the noise resonance would then be given by the transverse relaxation rate.

An interesting blend of noise spectroscopy and the FM NMOR method (Subsection 4.B) was recently studied using nonlinear Faraday rotation on the RbD lines.⁷⁵ A balanced polarimeter could be configured to detect either optical rotation or ellipticity of the light transmitted through atomic vapor. Instead of the deliberate application of laser-frequency modulation at a given rate, the frequency noise inherent to diode lasers was relied on. The noise power at the output of the balanced polarimeter at a fixed frequency was observed as a function of the magnetic field. Resonant features were seen at $B = 0$ and at the values of B for which twice the Larmor frequency co-

incided with the observation frequency, i.e., the counterparts of the usual FM NMOR resonances.

7. CONCLUSIONS AND OUTLOOK

We have discussed the various dynamic, nonlinear, magneto-optical effects, including transient effects occurring when the experimental conditions are changed suddenly, and beat-resonance effects that result from modulation of an experimental parameter. We have attempted to bring together diverse experimental techniques—which can involve various modulation schemes, the “quantum” low- J limit or the “classical” high- J limit, and related phenomena such as CPT—and describe them from a common viewpoint.

The dynamic effects have many applications in atomic and molecular physics, allowing experimental methods that would be difficult to implement using steady-state effects. For example, polarization moments can be separately influenced and measured, allowing determination and exploitation of their various properties, such as differing relaxation rates. High-sensitivity magnetometry based on optical rotation can be performed with arbitrarily large magnetic fields. Also, the dynamic effects provide a robust technique for precise measurements of energy-level splittings, which makes them an invaluable tool for fundamental symmetry tests relating to atomic and molecular structure and interactions.

APPENDIX A: POLARIZATION MOMENTS AND THE ANGULAR-MOMENTUM-PROBABILITY DISTRIBUTION

Here we describe in more detail the complementary descriptions of the polarization state discussed in Section 2. Most of the formulas given here can be found in the literature (for example, in Ref. 76), but they can be difficult to piece together, and, in particular, a discussion of the connection between the quantum and classical limits is not readily available. Thus it seems useful to gather together this information. In this Appendix equation numbers of formulas found in Ref. 76 are referred to in brackets.

To describe the polarization state of a particle, it can be helpful to write the state as a sum of tensor operators having the symmetries of the spherical harmonics $Y_{\kappa q}(\theta, \phi)$. This multipole expansion is useful not only for understanding the polarization symmetry (Fig. 2), but also for reducing the complexity of the density-matrix-evolution equations, especially for states with large angular momentum. In molecular spectroscopy, one typically deals with states of much larger angular momenta ($J \approx 100$) than with atoms. In this case, the standard Liouville equations of motion⁷⁷ form a large coupled system that can be difficult to solve. However, the equations of motion for the multipole expansion coefficients can be much simpler.¹⁰ This idea was introduced by Ducloy⁷⁸ and later applied to the analysis of a large variety of nonlinear magneto-optical effects in diatomic molecules (see Ref. 2 and references therein).⁷⁹

We employ the polarization operators \mathcal{T}_q^κ , defined to be irreducible tensors of rank κ that satisfy the normalization condition [Eq. 2.4(2)]:

$$\text{Tr } \mathcal{T}_q^{\kappa\dagger} \mathcal{T}_{q'}^\kappa = \delta_{\kappa\kappa'} \delta_{qq'} \quad (\text{A1})$$

and the phase relation [Eq. 2.4(3)]

$$\mathcal{T}_q^{\kappa\dagger} = (-1)^q \mathcal{T}_{-q}^\kappa. \quad (\text{A2})$$

Matrix elements of \mathcal{T}_q^κ resulting from this definition are given by [Eq. 2.4(8)]

$$\langle Jm' | \mathcal{T}_q^\kappa | Jm \rangle = \left(\frac{2\kappa + 1}{2J + 1} \right)^{1/2} \langle Jm \kappa q | Jm' \rangle, \quad (\text{A3})$$

where $\langle \dots | \dots \rangle$ are the Clebsch–Gordan coefficients. The density matrix is defined as $\rho = \overline{\Psi\Psi^\dagger}$, where Ψ is the wave function of one particle and the overbar denotes the average over the ensemble. It [or any arbitrary $(2J + 1)(2J + 1)$ Hermitian matrix] can be expanded in terms of the polarization operators as [Eq. 6.1(47)]

$$\rho = \sum_{\kappa=0}^{2J} \sum_{q=-\kappa}^{\kappa} \rho_q^\kappa \mathcal{T}_q^{\kappa\dagger}, \quad (\text{A4})$$

where the expansion coefficients ρ_q^κ are the expectation values of \mathcal{T}_q^κ [Eq. 6.1(48)]:

$$\rho_q^\kappa = \text{Tr } \rho \mathcal{T}_q^\kappa. \quad (\text{A5})$$

In terms of the density-matrix elements $\rho_{mm'}$ this gives [Eq. 6.1(49)]

$$\rho_q^\kappa = \left(\frac{2\kappa + 1}{2J + 1} \right)^{1/2} \sum_{m,m'=-J}^J \langle Jm \kappa q | Jm' \rangle \rho_{mm'}, \quad (\text{A6})$$

with the inverse transformation [Eq. 6.1(50)]

$$\rho_{mm'} = \sum_{\kappa=0}^{2J} \sum_{q=-\kappa}^{\kappa} \left(\frac{2\kappa + 1}{2J + 1} \right)^{1/2} \langle Jm \kappa q | Jm' \rangle \rho_q^\kappa. \quad (\text{A7})$$

These relations are also commonly written in an equivalent form using the identity

$$\langle Jm \kappa q | Jm' \rangle = (-1)^{J-m} \left(\frac{2J + 1}{2\kappa + 1} \right)^{1/2} \langle Jm' J - m | \kappa q \rangle. \quad (\text{A8})$$

To produce a visual representation of the polarization state, we plot the probability of the maximum projection of angular momentum along the unit vector $\hat{\mathbf{n}}_{(\theta, \phi)}$, i.e., the matrix element $\rho_{JJ}(\theta, \phi) = \langle \mathbf{J} \cdot \hat{\mathbf{n}}_{(\theta, \phi)} | \rho | \mathbf{J} \cdot \hat{\mathbf{n}}_{(\theta, \phi)} \rangle$, where [Eq. 6.1(20)]

$$\begin{aligned} |Jm_{(\theta, \phi)}\rangle &= \mathcal{D}(\phi, \theta, 0) |Jm\rangle, \\ &= \sum_{m'} D_{m'm}^J(\phi, \theta, 0) |Jm'\rangle \end{aligned} \quad (\text{A9})$$

are the eigenfunctions of the $\mathbf{J} \cdot \hat{\mathbf{n}}_{(\theta, \phi)}$ operator; the Wigner D -functions $D_{m'm}^J(\alpha, \beta, \gamma)$ are the matrix elements of the rotation operator $\mathcal{D}(\alpha, \beta, \gamma)$. Since the diagonal matrix elements of the polarization operators are

found from Eqs. (A3) and (A9) and the properties of the D -functions to be [Eq. 6.1(27)]

$$\begin{aligned} \langle Jm_{(\theta,\phi)} | T_q^\kappa | Jm_{(\theta,\phi)} \rangle \\ = \left(\frac{4\pi}{2J+1} \right)^{1/2} \langle Jm\kappa 0 | Jm \rangle Y_{\kappa q}(\theta, \phi), \end{aligned} \quad (\text{A10})$$

it can be seen from the expansion (A4) that the angular-momentum-probability distribution

$$\rho_{JJ}(\theta, \phi) = (2J)! \sum_{m\mu} \frac{\exp(i\mu\phi) [\cos(\theta/2)]^{2(J+m)} [\sin(\theta/2)]^{2(J-m)} \rho_{m+\mu/2, m-\mu/2}}{[(J-m-\mu/2)!(J+m-\mu/2)!(J-m+\mu/2)!(J+m+\mu/2)!]^{1/2}}. \quad (\text{A13})$$

$$\begin{aligned} \rho_{JJ}(\theta, \phi) &= \left(\frac{4\pi}{2J+1} \right)^{1/2} \\ &\times \sum_{\kappa=0}^{2J} \sum_{q=-\kappa}^{\kappa} \langle Jm\kappa 0 | JJ \rangle \rho_q^\kappa Y_{\kappa q}^*(\theta, \phi) \end{aligned} \quad (\text{A11})$$

is a linear combination of spherical harmonics $Y_{\kappa q}^*(\theta, \phi)$ with coefficients determined by the amplitude of the cor-

$$\rho_{JJ}(\theta, \phi) \approx \frac{(2J)!}{4^J} \sum_{\mu} \frac{(1-m/J)^{J-m} (1+m/J)^{J+m} \exp(i\mu\phi) \rho_{m+\mu/2, m-\mu/2}}{[(J-m-\mu/2)!(J+m-\mu/2)!(J-m+\mu/2)!(J+m+\mu/2)!]^{1/2}}. \quad (\text{A15})$$

responding polarization moment in the polarization state of the ensemble. Given a probability distribution $\rho_{JJ}(\theta, \phi)$, the polarization moments ρ_q^κ and thus the density-matrix elements $\rho_{mm'}$ can be recovered using the orthonormality of the spherical harmonics, so all three are complete and equivalent descriptions of the ensemble-averaged polarization. All three descriptions can be use-

$$\frac{(2J)!}{4^J} \frac{(1-m/J)^{J-m} (1+m/J)^{J+m}}{[(J-m-\mu/2)!(J+m-\mu/2)!(J-m+\mu/2)!(J+m+\mu/2)!]^{1/2}} \approx \frac{(2J)!}{4^J} \frac{(1-m/J)^{J-m} (1+m/J)^{J+m}}{(J-m)!(J+m)!} \approx 1. \quad (\text{A16})$$

ful in calculations, especially in the large- J limit, for which $\rho_{JJ}(\theta, \phi)$ corresponds (apart from a normalization factor²) to the classical probability distribution of the angular momentum direction.

For large angular momentum the expression for $\rho_{JJ}(\theta, \phi)$ in terms of the density-matrix elements $\rho_{mm'}$ is simplified considerably.^{83,84} From Eq. (A9) we have

$$\begin{aligned} \rho_{JJ}(\theta, \phi) &= \langle JJ_{(\theta,\phi)} | \rho | JJ_{(\theta,\phi)} \rangle \\ &= \sum_{m_1 m_2} D_{m_1 J}^{J*} D_{m_2 J}^J \rho_{m_1 m_2} \\ &= \sum_{m\mu} D_{m+\mu/2, J}^{J*} D_{m-\mu/2, J}^J \rho_{m+\mu/2, m-\mu/2}, \end{aligned} \quad (\text{A12})$$

where we have used the substitution $m_{1,2} = m \pm \mu/2$. The D -functions can be evaluated for the special case of interest here [Eq. 4.17(8)], giving

The factor depending on θ can be written

$$\begin{aligned} &[\cos(\theta/2)]^{2(J+m)} [\sin(\theta/2)]^{2(J-m)} \\ &= [1/4(1-\cos\theta)^{1-m/J} (1+\cos\theta)^{1+m/J}]^J, \end{aligned} \quad (\text{A14})$$

and for large J has a sharp peak centered at $\cos\theta = m/J$. Thus as $J \rightarrow \infty$, for a given θ only the term $m = J \cos\theta$ contributes to the sum, and we can write

For physical situations of interest we can assume that only a limited number of polarization moments are present ($\kappa \ll 2J$), which implies that only density-matrix elements $\rho_{m+\mu/2, m-\mu/2}$ with $\mu/2 \ll J$ are nonzero. For these terms in the sum, the factor with explicit dependence on J can be simplified using Stirling's approximation $n! \approx n^n e^{-n}$:

Thus in this limit we have

$$\rho_{JJ}(\theta, \phi) \approx \sum_{\mu} \exp(i\mu\phi) \rho_{m+\mu/2, m-\mu/2}. \quad (\text{A17})$$

For example, if one uses linearly polarized light to excite a molecular transition between states with the same J in the ground and excited state (Q -type transition) in the ab-

sence of a magnetic field, only diagonal density-matrix elements will be nonzero. We can calculate these matrix elements according to the simple formula⁸

$$\rho_{mm} = 3m^2/J(J+1)(2J+1). \quad (\text{A18})$$

Only one summand is left in Eq. (A17). Using $m = J \cos \theta$ we immediately get

$$\rho_{JJ}(\theta, \phi) \approx 3 \cos^2 \theta / 2J + 1. \quad (\text{A19})$$

The first three authors can be reached by e-mail at ealex@online.ru, mauzins@latnet.lv, and budker@socrates.berkeley.edu, respectively.

REFERENCES AND NOTES

- D. Budker, W. Gawlik, D. F. Kimball, S. M. Rochester, V. V. Yashchuk, and A. Weis, "Resonant nonlinear magneto-optical effects in atoms," *Rev. Mod. Phys.* **74**, 1153–1201 (2002).
- M. Auzinsh and R. Ferber, *Optical Polarization of Molecules* (Cambridge U. Press, Cambridge, UK, 1995).
- We will use the word "particle" to refer to either atoms or molecules.
- S. Haroche, "Quantum beats and time-resolved fluorescence spectroscopy," in *High-Resolution Laser Spectroscopy*, K. Shimoda, ed. (Springer, Berlin, 1976), pp. 256–313.
- J. N. Dodd and G. W. Series, "Time-resolved fluorescence spectroscopy," in *Progress in Atomic Spectroscopy*, W. Hanle and H. Kleinpoppen, eds. (Plenum, New York, 1978), Vol. 1, pp. 639–677.
- E. Hack and J. Huber, "Quantum-beat spectroscopy of molecules," *Int. Rev. Phys. Chem.* **10**, 287–317 (1991).
- E. B. Aleksandrov, M. P. Chaika, and G. I. Khvostenko, *Interference of Atomic States* (Springer-Verlag, New York, 1993).
- M. Auzinsh, "Angular momenta dynamics in magnetic and electric field: Classical and quantum approach," *Can. J. Phys.* **75**, 853–872 (1997).
- S. M. Rochester and D. Budker, "Atomic polarization visualized," *Am. J. Phys.* **69**, 450–454 (2001).
- M. P. Auzinsh and R. S. Ferber, "Optical pumping of diatomic molecules in the electronic ground state: classical and quantum approaches," *Phys. Rev. A* **43**, 2374–2386 (1991).
- M. Dyakonov, "Theory of resonance scattering of light by a gas in the presence of a magnetic field," *Zh. Eksp. Teor. Fiz.* **47**, 2213–2221 (1964) [*Sov. Phys. JETP* **20**, 1484–1489 (1965)].
- P. K. Majumder, B. J. Venema, S. K. Lamoreaux, B. R. Heckel, and E. N. Fortson, "Test of the linearity of quantum mechanics in optically pumped ²⁰¹Hg," *Phys. Rev. Lett.* **65**, 2931–2934 (1990).
- M. Auzinsh, "The evolution and revival structure of angular momentum quantum wave packets," *Can. J. Phys.* **77**, 491–503 (1999).
- E. Aleksandrov, "Luminescence beats induced by pulsed excitation of coherent states," *Opt. Spectrosc. (USSR)* **17**, 522–523 (1964).
- J. N. Dodd, R. Kaul, and D. Warrington, "The modulation of resonance fluorescence excited by pulsed light," *Proc. Phys. Soc. London, Sect. A* **84**, 176–178 (1964).
- W. Lange and J. Mlynek, "Quantum beats in transmission by time-resolved polarization spectroscopy," *Phys. Rev. Lett.* **40**, 1373–1375 (1978).
- J. M. Geremia, J. K. Stockton, A. C. Doherty, and H. Mabuchi, "Quantum Kalman filtering and the Heisenberg limit in atomic magnetometry," *Phys. Rev. Lett.* **91**, 25801 (2003).
- J. M. Geremia, J. K. Stockton, and H. Mabuchi, "Sub-shotnoise atomic magnetometry," (2004), <http://arxiv.org/abs/quant-ph/0401107>.
- M. O. Scully and M. S. Zubairy, *Quantum Optics* (Cambridge U. Press, Cambridge, UK, 1997).
- M. P. Auzinsh, D. Budker, D. F. Kimball, J. E. Stalnaker, A. O. Sushkov, and V. V. Yashchuk, "Can a quantum nondemolition measurement improve the sensitivity of an atomic magnetometer?" (2004), <http://arxiv.org/abs/physics/0403097>.
- The quantum-beat frequency must be higher than the relaxation rate for quantum-beat dynamics to be clearly observed. In molecules, for example, the excited-state relaxation rate is often dominated by radiative decay and is typically $\sim 10^8 \text{ s}^{-1}$, which is greater than the typical ground-state relaxation rate ($\sim 10^6 \text{ s}^{-1}$). Thus larger magnetic fields are required to observe excited-state Zeeman beats than for the observation of ground-state quantum beats.
- M. P. Auzinsh, R. S. Ferber, and I. Pirags, "K₂ ground-state relaxation studies from transient process kinetics," *J. Phys. B* **16**, 2759–2771 (1983).
- The idea of stroboscopic matching to increase coupling between systems (light and precessing spins in this context) is also omnipresent in the field of nuclear magnetic resonance. For example, Hahn and co-workers introduced various methods of coupling spin systems with different gyromagnetic ratios together by matching the Larmor frequency of one system to the Rabi frequency of the other (Kaplan–Hahn matching) or by matching the Rabi frequencies of the two systems (Hartmann–Hahn matching).²⁴ A general review²⁵ of the connection between concepts in quantum optics and nuclear magnetic resonance was given by Hahn.
- C. P. Slichter, *Principles of Magnetic Resonance*, Springer Series in Solid-State Sciences (Springer, New York, 1996).
- E. L. Hahn, "Concepts of NMR in quantum optics," *Concepts Magn. Reson.* **9**, 69–81 (1997).
- W. Bell and A. Bloom, "Optically driven spin precession," *Phys. Rev. Lett.* **6**, 280–281 (1961).
- W. Bell and A. Bloom, "Observation of forbidden resonances in optically driven spin systems," *Phys. Rev. Lett.* **6**, 623–624 (1961).
- E. B. Aleksandrov, "Quantum beats of luminescence under modulated light excitation," *Opt. Spectrosc.* **14**, 233–234 (1963).
- M. Auzinsh, "Nonlinear phase resonance of quantum beats in the dimer ground state," *Opt. Spectrosc. (USSR)* **68**, 750–752 (1990).
- R. S. Ferber, A. I. Okunevich, O. A. Shmit, and M. Y. Tamanis, "Landé factor measurements for the ¹³⁰Te₂ electronic ground state," *Chem. Phys. Lett.* **90**, 476–480 (1982).
- M. Auzinsh, K. Nasyrov, M. Tamanis, R. Ferber, and A. Shalagin, "Resonance of quantum beats in a system of magnetic sublevels of the electronic ground state of molecules," *Sov. Phys. JETP* **65**, 891–897 (1987).
- M. P. Auzinsh, K. A. Nasyrov, M. Y. Tamanis, R. S. Ferber, and A. M. Shalagin, "Determination of the ground-state Landé factor for diatomic molecules by a beat-resonance method," *Chem. Phys. Lett.* **167**, 129–136 (1990).
- J. P. Jacobs, W. M. Klipstein, S. K. Lamoreaux, B. R. Heckel, and E. N. Fortson, "Limit on the electric-dipole moment of ¹⁹⁹Hg using synchronous optical pumping," *Phys. Rev. A* **52**, 3521–3540 (1995).
- M. V. Romalis, W. C. Griffith, J. P. Jacobs, and E. N. Fortson, "New limit on the permanent electric dipole moment of ¹⁹⁹Hg," *Phys. Rev. Lett.* **86**, 2505–2508 (2001).
- M. V. Romalis, W. C. Griffith, J. P. Jacobs, and E. N. Fortson, "Art and Symmetry in Experimental Physics: Festschrift for Eugene D. Commins," in *AIP Conference Proceedings, Vol. 596*, D. Budker, S. J. Freedman, and P. Bucksbaum, eds. (American Institute of Physics, Melville, N.Y., 2001), pp. 47–61.
- D. Budker, D. F. Kimball, V. V. Yashchuk, and M. Zolotarev, "Nonlinear magneto optical rotation with frequency-modulated light," *Phys. Rev. A* **65**, 055403 (2002).
- V. V. Yashchuk, D. Budker, W. Gawlik, D. F. Kimball, Y. P. Malakyan, and S. M. Rochester, "Selective addressing of high-rank atomic polarization moments," *Phys. Rev. Lett.* **90**, 253001 (2003).

38. Y. P. Malakyan, S. M. Rochester, D. Budker, D. F. Kimball, and V. V. Yashchuk, "Nonlinear magneto-optical rotation of frequency-modulated light resonant with a low- J transition," *Phys. Rev. A* **69**, 013817 (2004).
39. E. B. Aleksandrov, "Optical manifestation of interference of non-degenerate atomic states," *Sov. Phys. Usp.* **15**, 436–451 (1972).
40. D. Budker, D. F. Kimball, and V. V. Yashchuk, *Nonlinear Magneto-Optic Atomic Magnetometry for the Earth Field Range*, Technical Report LBNL PUB-5449, Lawrence Berkeley National Laboratory (1999).
41. J. Dupont-Roc, "Determination of the three components of a weak magnetic field by optical methods," *Rev. Phys. Appl.* **5**, 853–864 (1970).
42. H. Failache, P. Valente, G. Ban, V. Lorent, and A. Lezama, "Inhibition of electromagnetically induced absorption due to excited state decoherence in Rb vapor," *Phys. Rev. A* **67**, 043810 (2003).
43. A. I. Okunevich, "Parametric relaxation resonance of optically oriented atoms in a transverse magnetic field," *Zh. Eksp. Teor. Fiz.* **66**, 1578–1580 (1974).
44. L. Novikov, "Optically excited parametric resonance," *C. R. Seances Acad. Sci., Ser. B* **278**, 1063–1065 (1974).
45. A. I. Okunevich, "Parametric relaxation resonance of optically oriented metastable ^4He atoms in an effective magnetic field," *Zh. Eksp. Teor. Fiz.* **67**, 881–889 (1974).
46. E. B. Aleksandrov, M. V. Balabas, and V. A. Bonch-Bruевич, "Nutation caused by a change in relaxation rate," *Pis'ma Zh. Eksp. Teor. Fiz.* **45**, 309–310 (1987).
47. E. Arimondo, in *Progress in Optics*, Vol. XXXV, E. Wolf, ed. (Elsevier, New York, 1996), pp. 259–354.
48. C. Andreeva, G. Bevilacqua, V. Biancalana, S. Cartaleva, Y. Dancheva, T. Karaulanov, C. Marinelli, E. Mariotti, and L. Moi, "Two-color coherent population trapping in a single Cs hyperfine transition, with application in magnetometry," *Appl. Phys. B* **76**, 667–675 (2003).
49. D. Suter, T. Marty, and H. Klepel, "Rotation properties of multipole moments in atomic sublevel spectroscopy," *Opt. Lett.* **18**, 531–533 (1993).
50. D. Suter and T. Marty, "Experimental observation of the rotation properties of atomic multipoles," *J. Opt. Soc. Am. B* **11**, 242–252 (1994).
51. J. D. Xu, G. Wäckerle, and M. Mehring, "Multiple-quantum spin coherence in the ground state of alkali atomic vapors," *Phys. Rev. A* **55**, 206–213 (1997).
52. J. D. Xu, G. Wäckerle, and M. Mehring, "Optical detection of spin multipole order in the ground state of alkali atoms," *Z. Phys. D* **42**, 5–13 (1997).
53. A. B. Matsko, I. Novikova, G. R. Welch, and M. S. Zubairy, "Enhancement of Kerr nonlinearity by multiphoton coherence," *Opt. Lett.* **28**, 96–98 (2003).
54. B. Łobodziński and W. Gawlik, "Multipole moments and trap states in forward scattering of resonance light," *Phys. Rev. A* **54**, 2238–52 (1996).
55. B. Łobodziński and W. Gawlik, "Role of trap states in forward scattering of resonance light," *Phys. Scr.* **T70**, 138–44 (1997).
56. D. Budker, D. F. Kimball, S. M. Rochester, V. V. Yashchuk, and M. Zolotarev, "Sensitive magnetometry based on nonlinear magneto-optical rotation," *Phys. Rev. A* **62**, 043403 (2000).
57. C. Cohen-Tannoudji, J. DuPont-Roc, S. Haroche, and F. Lalö, "Detection of the static magnetic field produced by the oriented nuclei of optically pumped ^3He gas," *Phys. Rev. Lett.* **22**, 758–760 (1969).
58. B. Cheron, H. Gilles, J. Hamel, O. Moreau, and E. Noel, "A new optical pumping scheme using a frequency modulated semi-conductor laser for ^4He magnetometers," *Opt. Commun.* **115**, 71–74 (1995).
59. B. Cheron, H. Gilles, J. Hamel, O. Moreau, and E. Noel, " ^4He optical pumping with frequency modulated light," *J. Phys. II* **6**, 175–185 (1996).
60. H. Gilles, J. Hamel, and B. Cheron, "Laser pumped ^4He magnetometer," *Rev. Sci. Instrum.* **72**, 2253–2260 (2001).
61. V. V. Yashchuk, J. Granwehr, D. F. Kimball, S. M. Rochester, A. Trabesinger, J. T. Urban, D. Budker, and A. Pines, "Hyperpolarized xenon nuclear spins detected by optical atomic magnetometry" (2004), <http://arxiv.org/abs/physics/0404090>.
62. M. P. Auzinsh, M. Y. Tamanis, and R. S. Ferber, "Observation of quantum beats in the kinetics of the thermalization of diatomic molecules in the electronic ground state," *JETP Lett.* **42**, 160–163 (1985).
63. M. Auzinsh, M. Tamanis, and R. Ferber, "Zeeman quantum beats after optical depopulation of the ground electronic state of diatomic molecules," *Sov. Phys. JETP* **63**, 688–693 (1986).
64. H. Lefebvre-Brion and R. W. Field, *The Spectra and Dynamics of Diatomic Molecules*, 2nd ed. (Academic, New York, 2004).
65. M. Auzinsh and R. Ferber, "Observation of quantum-beat resonance between magnetic sublevels with $\Delta M = 4$," *JETP Lett.* **39**, 452–455 (1984).
66. R. Wallenstein, J. A. Paisner, and A. L. Schawlow, "Observation of Zeeman quantum beats in molecular iodine," *Phys. Rev. Lett.* **32**, 1333–1336 (1974).
67. B. C. Regan, D. Commins, C. J. Schmidt, and D. DeMille, "New limit on the electron electric dipole moment," *Phys. Rev. Lett.* **88**, 071805 (2002).
68. D. DeMille, F. Bay, S. Bickman, B. Kawall, L. Hunter, J. Krause, D., S. Maxwell, and K. Ulmer, "Search for the electric dipole moment of the electron using metastable PbO ," in *AIP Conference Proceedings*, D. Budker, P. Bucksbaum, and S. J. Freedman, eds. (American Institute of Physics, Melville, N.Y., 2001), Vol. 596, pp. 72–83.
69. G. Herzberg, *Spectra of Diatomic Molecules* (Krieger, Malabar, Fla., 1989).
70. D. Kawall, F. Bay, S. Bickman, Y. Jiang, and D. DeMille, "Precision Zeeman-Stark spectroscopy of the metastable $\alpha(1)[^3\Sigma^+]$ state of PbO ," *Phys. Rev. Lett.* **92**, 133007 (2004).
71. S. Rochester, C. J. Bowers, D. Budker, D. DeMille, and M. Zolotarev, "Measurement of lifetimes and tensor polarizabilities of odd-parity states of atomic samarium," *Phys. Rev. A* **59**, 3480–3494 (1999).
72. D. Budker, D. DeMille, E. D. Commins, and M. S. Zolotarev, "Experimental investigation of excited states in atomic dysprosium," *Phys. Rev. A* **50**, 132–143 (1994).
73. A. T. Nguyen, D. Budker, D. DeMille, and M. Zolotarev, "Search for parity nonconservation in atomic dysprosium," *Phys. Rev. A* **56**, 3453–3463 (1997).
74. E. B. Aleksandrov and V. S. Zapasskii, "Magnetic resonance in the Faraday rotation noise spectrum," *Zh. Eksp. Teor. Fiz.* **81**, 132–138 (1981).
75. M. Martinelli, P. Valente, H. Failache, D. Felinto, L. S. Cruz, P. Nussenzweig, and A. Lezama, "Noise spectroscopy of non-linear magneto-optical resonances in Rb vapor," *Phys. Rev. A* **69**, 043809, (2004).
76. D. A. Varshalovich, A. N. Moskalev, and V. K. Khersonskii, *Quantum Theory of Angular Momentum: Irreducible Tensors, Spherical Harmonics, Vector Coupling Coefficients, 3nj Symbols* (World Scientific, Singapore, 1988).
77. L. Allen and J. H. Eberly, *Optical Resonance and Two-Level Atoms* (Dover, New York, 1987).
78. M. Ducloy, "Non-linear effects in optical pumping with lasers. I. General theory of the classical limit for levels of large angular momenta," *J. Phys. B* **9**, 357–381 (1976).
79. When the excitation light has a spectral profile broader than the homogeneous absorption linewidth, calculations can also be simplified by using rate equations for the Zeeman coherences.^{80,81} It has been demonstrated that in many cases these rate equations give very good agreement between the model and experimental results. Recently, a detailed analysis⁸² of the application limits for the rate equations for Zeeman coherences for nonlinear magneto-optical effects was carried out.
80. C. Cohen-Tannoudji, "Theorie quantique du cycle de pompage optique. Verification experimentale des nouveaux effets prevus (1-re partie)," *Ann. Phys. (Paris)* **7**, 423–461 (1962).
81. C. Cohen-Tannoudji, "Theorie quantique du cycle de

- pompage optique. Verification experimentale des nouveaux effets prevus (2-e partie)," *Ann. Phys. (Paris)* **7**, 469–504 (1962).
82. K. Blushs and M. P. Auzinsh, "Validity of rate equations for Zeeman coherences for analysis of nonlinear interaction of atoms with laser radiation," *Phys. Rev. A* **69**, 063806 (2004).
83. K. A. Nasyrov and A. M. Shalagin, "Interaction between intense radiation and atoms or molecules experiencing classical rotary motion," *Zh. Eksp. Teor. Fiz.* **81**, 6649–6663 (1981).
84. K. A. Nasyrov, "Wigner representation of rotational motion," *J. Phys. A* **32**, 6663–6678 (1999).